TRANSPORT IN MOSFET'S, MODFET'S AND HEMT'S

Erasmus Langer and Siegfried Selberherr,

Institute for Microelectronics,
Technical University Vienna,
Gußhausstraße 27–29, A–1040 WIEN, Austria

ABSTRACT

This contribution is intended to review the state-of-the-art in numerical simulation of particular transistor devices within our institute. Much emphasis is laid on the discussion of recent refinements to the carrier transport model which primarily is based on the so–called enhanced drift–diffusion equations with two essential extensions: On the one hand, carrier heating properly is taken into account using the Monte Carlo method (hybrid model), and on the other hand the one dimensional Schrödinger equation is introduced for the simulation of the charge–control in order to obtain satisfactory results for strained–layer Si/Ge heterostructure devices. The presented procedure leads to the self–consistent inclusion of quantum–mechanical effects in the simulation. Simulation results of miniaturized MOS transistors are discussed which have been obtained by our simulator MINIMOS.

1. INTRODUCTION

Since 1960 when the demonstration of the practically usable MOS transistor took place [24] its development has shown to evolve dramatically. Today, about thirty years later, integrated circuits with millions of devices per single chip are manufactured. In order to minimize the number of cycles of trial and error in device fabrication improved understanding of basic device operation has attained crucial importance. Thus, numerical modeling of MOS transistors has become a basic requirement for the development of prototype devices.

The numerical simulation of semiconductor devices represents a very large field. Since the probably first publication concerning a two–dimensional solution of the Poisson equation with application to a MOS structure by Loeb et al. [32] and Schroeder and Muller [41] in 1968 a lot of work has been contributed with basically two different aims: On the one hand, the numerical tools have been extended in order to obtain globally more detailed information (transient simulation, e.g.: [12], [18], [25] as well as extension to three spatial dimensions, e.g.: [8], [31], [44]). On the other hand, either the models of physical parameters have been improved, e.g.: [29], [43], [45], [46], [49], or special physical effects have been investigated, e.g.: [15], [20], [36], [37], or the mathematical model of the carrier transport in semiconductors has been refined, e.g.: [27], [40]. This paper mainly deals with the latter. A transport model suitable for MOSFET's, MODFET's and HEMT's will be presented.

2. EXTENDED HYBRID TRANSPORT MODEL

The state-of-the-art in semiconductor technology enables the fabrication of semiconductor devices with characteristic lengths smaller than 1 μm in an industrial environment. Such devices are characterized by very large electric fields and rapid spatial variations of the electric field and carrier concentrations. These variations occur over a distance comparable with the characteristic lengths of carrier transport, i.e. the average momentum relaxation length and the energy relaxation length. Owing to the very large electric fields the assumption of small perturbations around equilibrium breaks down which the drift–diffusion transport model is based on. It was realized long ago that a straightforward extension of the classical semiconductor equations would have to include the energy balance of field–driven carriers [9]. One way for this purpose is an enhanced drift–diffusion model which accounts for the energy balance. The obvious benefit of this approach is that it can be implemented without great efforts in an existing simulation program based on the basic semiconductor equations. Another practicable way to include hot carrier effects is the usage of the hydrodynamic model [39] which implies the energy conservation equation. Last not least, there is to mention the Monte Carlo method whose most important drawback is — as usual — the enormous amount of required computing resources.

2.1. Enhanced Drift–Diffusion Equations

Starting point for our refinement of the transport model are the so–called "Enhanced drift–diffusion equations" consisting of Poisson's equation (1), con-

tinuity equations for electrons and holes (2), (3), and the current relations for both carrier types (4), (5).

$$\operatorname{div}(\varepsilon \cdot \operatorname{grad} \psi) = -\rho \tag{1}$$

$$\operatorname{div} \vec{J}_n - q \cdot \frac{\partial n}{\partial t} = q \cdot R \tag{2}$$

$$\operatorname{div} \vec{J}_p + q \cdot \frac{\partial p}{\partial t} = -q \cdot R \tag{3}$$

$$\vec{J}_n = q \cdot \mu_n \cdot n \cdot \left(\vec{E} + \frac{1}{n} \cdot \operatorname{grad} \left(n \cdot \frac{k_B \cdot T_n}{q} \right) \right) \tag{4}$$

$$\vec{J}_p = q \cdot \mu_p \cdot p \cdot \left(\vec{E} - \frac{1}{p} \cdot \operatorname{grad} \left(p \cdot \frac{k_B \cdot T_p}{q} \right) \right) \tag{5}$$

At the first glance these equations look like the fundamental semiconductor equations which have already been used in the famous work of Gummel in 1964 [13]. The enhancement lies in the existence of different temperatures T_n and T_p within the diffusion terms of the current relations (4), (5) as well as in the appropriate models for the carrier mobilities μ_n and μ_p which will be shown in the next section. The solution of the enhanced drift–diffusion equations accounts for hot–carrier transport in semiconductors [16]. An adequate model for already existing simulation programs has been implemented first in MINIMOS [17], our tool for the two and three dimensional analysis of miniaturized MOS transistors.

2.2. Hybrid Transport Model

Since the very first beginning of Monte Carlo simulations in the field of carrier transport in semiconductor devices [34] the most important drawback up to now is the enormous amount of computing resources required by this method for the solution of the Boltzmann transport equation (6) where $f = f(x_j, u_j, t)$ is the distribution function, x_j, u_j $(j = 1,2,3)$ are the components of the vector position $\vec{x}$ and group velocity $\vec{u}$, q is the electron charge, m denotes the effective mass of the carriers under investigation, $\vec{E}$ is the electric field, and C denotes the collision integral.

$$\frac{\partial f}{\partial t} + \vec{u} \cdot \operatorname{grad}_x f \pm \frac{q}{m} \cdot \vec{E} \cdot \operatorname{grad}_u f = C \tag{6}$$

The main benefits of this method are the facts that it is simple to implement, that sophisticated physical models can be used, and that any desired physical information can easily be extracted [22].

A very promising way is the coupling of the Monte Carlo method and the drift–diffusion equations [27] which is based on the following considerations: The Monte Carlo method is well suited to describe the non–equilibrium transport occurring under conditions appearing in ultra small MOS transistors (i.e. very high electric field in the active region with rapid changes over distances comparable to the mean free path of the carriers). On the other hand, for the description of low field transport the drift–diffusion model with local transport coefficients provides sufficient accuracy. Moreover, the drift–diffusion model has turned out to be even superior to the Monte Carlo method in regions with retarded fields. Therefore, several attempts were published to combine the drift–diffusion and Monte Carlo technique in order to benefit from the different capabilities of both methods [38], [47]. In the following, a recently performed implementation of the hybrid transport model in the existing simulation tool MINIMOS shall be discussed.

Three–dimensional scattering rates in the entire device are assumed, thus neglecting quantization effects eventually occurring in an inversion layer. Multiplication of the Boltzmann transport equation with wave vector component k_i and integration of $\vec{k}$ leads to a momentum balance equation, which reads for electrons

$$-\left(q \cdot E_i + \tfrac{1}{n} \textstyle\sum_{j=1}^{2} \frac{\partial (n \cdot (\hbar \cdot k_i \cdot v_j))}{\partial x_j}\right) = \left\langle \int (\hbar \cdot k_i - \hbar \cdot k_i') \cdot S(\vec{k}, \vec{k}') \cdot \mathrm{d}^3 \vec{k}' \right\rangle, \; i = 1,2 \tag{7}$$

where v denotes the group velocity. (It should be mentioned that in the following the index n for indicating the electrons is omitted as this carrier type is discussed in this section only.) The average operator $\langle A \rangle$ is the mean value of $A(\vec{k})$ weighted by the local distribution function $f(\vec{x}, \vec{k})$. The left hand side can be interpreted as driving force that acts on the electron ensemble, consisting of the electric field plus diffusion term, whereas the right hand side describes the rate of momentum loss due to scatterings. This equation can be expressed in a form similar to the drift–diffusion current relation. The parameters needed in this current relation are derived in the following way. For band structures with spheric and ellipsoidal energy surfaces the vector valued momentum loss integral is colinear with the momentum $\hbar \vec{k}$

$$\int (\hbar \cdot \vec{k} - \hbar \cdot \vec{k}') \cdot S(\vec{k}, \vec{k}') \cdot \mathrm{d}^3 \vec{k}' = \hbar \cdot \vec{k} \cdot \lambda_{\mathrm{m}}(E). \tag{8}$$

Here the proportionality factor $\lambda_{\mathrm{m}}(E)$ is the momentum scattering rate. With the local average velocity the local momentum loss mobility can be defined as

$$\mu = q \cdot \frac{\| \langle \vec{v} \rangle \|}{\| \langle \hbar \cdot \vec{k} \cdot \lambda_{\mathrm{m}}(E) \rangle \|} \tag{9}$$

where $\|B\|$ denotes the maximum norm of B. This definition does not rely on the relaxation time approximation and, since no effective mass occurs in this formula, extension to general bands is straightforward. In the latter case μ would have tensor property. The definition of the thermal voltage tensor (which is proportional to the temperature tensor: $U_{ij} = (k_B/q) T_{ij}$) results directly from the momentum

conservation equation (7)

$$U_{ij} = \frac{1}{q} \cdot \langle \hbar \cdot k_i \cdot v_j \rangle . \qquad (10)$$

This definition is independent of the underlying band structure model. Inserting these definitions in (7) one obtains a general current relation

$$J_i = q \cdot n \cdot \mu \cdot \left(E_i + \frac{1}{n} \cdot \sum_{j=1}^{2} \frac{\partial (n \cdot U_{ij})}{\partial x_j} \right) . \qquad (11)$$

The differences between this current relation and the classical one are twofold. Firstly, the diffusion term is more complicated owing to the tensor property of the thermal voltage. Secondly, the parameters μ and U_{ij} can no longer be treated simply as parameters depending on electric field or other local quantities — as it is usually done in the conventional drift–diffusion model — because they carry information of the local distribution function. By means of the Monte Carlo method these parameters are evaluated. The conventional simulator using the Monte Carlo parameters $\mu(\vec{x})$ and $U_{ij}(\vec{x})$ in the current relation (11) is then capable of recovering the Monte Carlo results for $n(\vec{x})$ and $\vec{J}_n(\vec{x})$. In this way hot electron effects, such as velocity overshoot and hot carrier diffusion, are consistently included in the conventional simulator. The solution is performed globally in the whole device, but only in the high field region mobility and temperature profiles have to be extracted from the Monte Carlo procedure. In regions with low fields and low spatial inhomogeneities local models can be used thus saving computation time.

The continuity equation in conjunction with a drift–diffusion current relation employing a scalar temperature yields an elliptic partial differential equation which has diagonal form. If an anisotropic temperature is taken into account cross derivatives appear in the elliptic operator. Conventional device simulators solve elliptic systems which are in diagonal form, therefore a scalar temperature is desirable. Neglecting the off diagonal elements in (10) a scalar temperature is used which is the arithmetic mean value of the main diagonal elements.

For the first conduction band of silicon we use a model consisting of six anisotropic valleys with a first order correction for nonparabolicity [23]. Acoustic intravalley scattering in the elastic approximation, intervalley phonon scattering, surface roughness scattering, and coulomb scattering are taken into account. Except of the latter one all mechanisms are isotropic. In the case of surface scattering in the inversion layer the wave vector is redistributed randomly in a plane parallel to the Si–SiO_2 interface. For isotropic scattering mechanisms the momentum scattering rate does not differ from the total scattering rate. The following

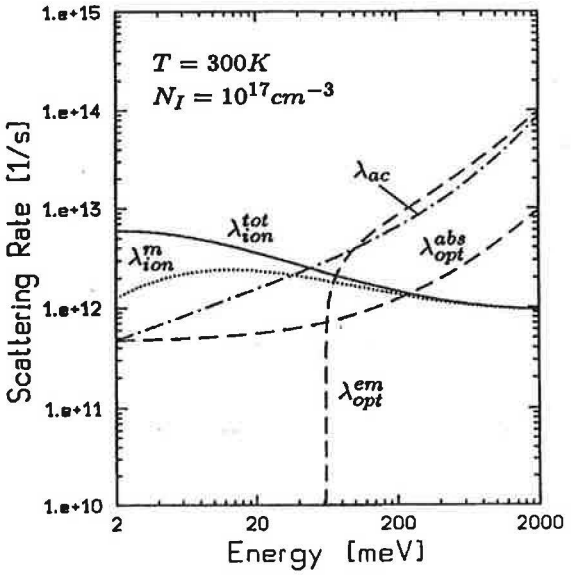

Figure 1: Total and momentum scattering rates used for mobility calculation.

superposition implies independence of all scattering processes

$$\lambda_{\mathrm{m}}(E) = \lambda_{\mathrm{ac}}^{\mathrm{tot}} + \lambda_{\mathrm{opt}}^{\mathrm{tot}} + \lambda_{\mathrm{surf}}^{\mathrm{tot}} + \lambda_{\mathrm{ion}}^{\mathrm{m}} . \qquad (12)$$

Coulomb interaction is the only one to be treated separately. The momentum loss integral (8) is evaluated by the Brooks–Herring formulation for the transition rate $S(\vec{k}, \vec{k}')$ and

$$\lambda_{\mathrm{ion}}^{\mathrm{m}}(E) = \lambda_{\mathrm{ion}}^{\mathrm{tot}} - \lambda_{\mathrm{ion}}'(E) \qquad (13)$$

is obtained. The subtraction corresponds to the difference of initial and final wave vector in (8).

Fig. 1 depicts the energy dependencies of total ($\lambda_{\mathrm{ion}}^{\mathrm{tot}}$) and momentum ($\lambda_{\mathrm{ion}}^{\mathrm{m}}$) scattering rate for ionized impurities, and additionally the total scattering rates for acoustic intravalley phonons (λ_{ac}) and one representative intervalley phonon mode (emission and absorption).

2.3. Actually performed improvements

Actually our transport model is refined to extend its simulation capability to strained-layer Si/Ge heterostructure devices such as the MODFET [10] or the quantum well MOSFET [35]. The improved transport model is also applicable to AlGaAs/GaAs heterostructure devices such as the high electron mobility transistor (HEMT) [14].

For this purpose we proceed in three steps:

- The appropriate geometrical constructs together with strain– and composition–dependent models for electrical permittivities, band offsets and heterodiscontinuities, as well as carrier mobilities [33] are implemented in MINIMOS. At this step, the hybrid transport model is already enabled.

- The simulation of the charge–control of the device involves the simultaneous solution of the one–dimensional Schrödinger and Poisson equation over the structure. The level of sophistication of the physical model employed in this part follows closely the approach in [21].
- The two previous steps are merged, thus leading to the self–consistent inclusion of quantum–mechanical effects in the simulation [50].

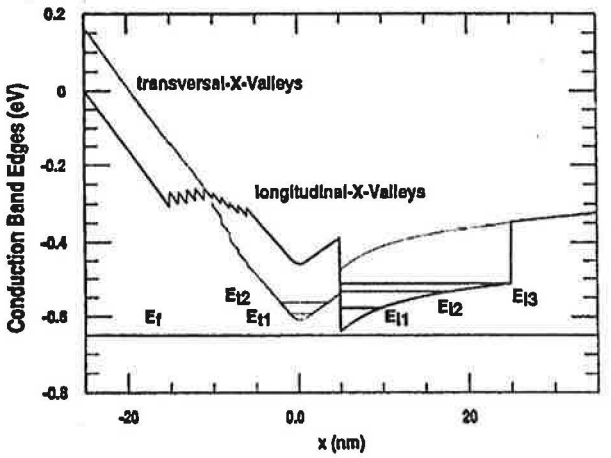

Figure 2: Conduction band edges of an n-MODFET

The one–dimensional Schrödinger equation reads

$$\left(-\frac{\hbar^2}{2m_z^*}\frac{d^2}{dz^2}+V(z)\right)\psi(z)=E_n\psi(z) \qquad (14)$$

where z is the coordinate perpendicular to the hetero–junction, ψ means the wave function, E_n is the n-th eigen energy, V the potential energy, and m_z^* is the effective mass perpendicular to the hetero–junction. In order to perform an adequate discretization the wave equation is rewritten according to

$$\psi''(z)=\left(\frac{2m^*}{\hbar^2}(V(z)-E_n)\right)\cdot\psi(z) \quad . \qquad (15)$$

As a first result, we present the calculated conduction band edge (Fig. 2) and quantum mechanical charge density (Fig. 3) for an n–MODFET similar to that described in [10]. It should be noted that the physical model used for the calculation of the envelope function accounts for the strain–split X valleys in the conduction band as well as for the strain dependence of the valence band lineups. These are assigned following the ab initio calculations in [48] and using deformation potential theory. Hole statistics is treated classically while dopant ionization is handled using Fermi–Dirac occupation statistics, whose neglect we believe can lead to significant differences. The graded layer is approximated in a step–wise fashion, leading to the spiked conduction band profile of Fig. 2. The

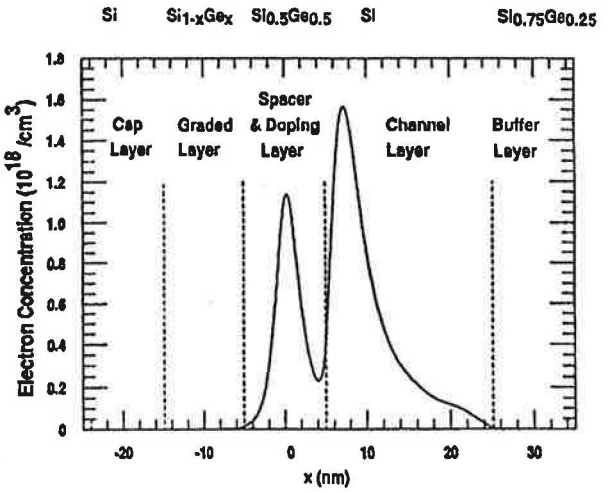

Figure 3: Free electron concentration in the same device

size of the parasitic channel near the doping spike is larger than in [21], probably due to the choice of a smaller value for the band offset in the longitudinal valleys and a larger value in the transversal ones.

3. MODELS FOR PARAMETERS

The fundamental semiconductor equations include a set of parameters which have to be appropriately modeled in order to describe the various transport phenomena qualitatively and quantitatively correctly. The basic requirement for an estimation of most of these physical parameters is independent more or less of the underlying transport model as the Poisson equation (1) and both continuity equations (2), (3) have to be solved self–consistently in any case. The physical parameters to be regarded are: the space charge ρ within the Poisson equation (1), the carrier generation/recombination term R which represents the right hand side of the continuity equations (2), (3), the carrier mobilities μ_n, μ_p, and the carrier temperatures T_n, T_p. Owing to lack of space, only the both latter will be discussed in the following as they are directly related to the enhanced drift–diffusion equations. Adequate models for the other physical parameters can be found in [28].

3.1. Modeling Carrier Mobilities

The models for the carrier mobilities have to take into account a great variety of scattering mechanisms the most basic one of which is lattice scattering. The lattice mobility in pure silicon can be fitted with simple power laws

$$\mu_n^L = 1430\frac{\mathrm{cm}^2}{\mathrm{Vs}}\cdot\left(\frac{T}{300\mathrm{K}}\right)^{-2}$$

$$\mu_p^L = 460\frac{\mathrm{cm}^2}{\mathrm{Vs}} \cdot \left(\frac{T}{300\mathrm{K}}\right)^{-2.18} . \qquad (16)$$

The expressions (16) fit well experimental data of [1], [5], and [30].

The next effect to be considered is ionized impurity scattering. The best established procedure for this task is to take the functional form (17) of the fit provided by Caughey and Thomas [7] and use temperature dependent coefficients.

$$\mu_{n,p}^{LI} = \mu_{n,p}^{min} + \frac{\mu_{n,p}^{L} - \mu_{n,p}^{min}}{1 + \left(\frac{CI}{C_{n,p}^{ref}}\right)^{\alpha_{n,p}}} \qquad (17)$$

$$\begin{aligned} \mu_n^{min} &= 80\frac{\mathrm{cm}^2}{\mathrm{Vs}} \cdot \left(\frac{T}{300\mathrm{K}}\right)^{-0.45} \\ \mu_p^{min} &= 45\frac{\mathrm{cm}^2}{\mathrm{Vs}} \cdot \left(\frac{T}{300\mathrm{K}}\right)^{-0.45} \end{aligned} \qquad (18)$$

$$\begin{aligned} C_n^{ref} &= 1.12 \cdot 10^{17}\mathrm{cm}^{-3} \cdot \left(\frac{T}{300\mathrm{K}}\right)^{3.2} \\ C_p^{ref} &= 2.23 \cdot 10^{17}\mathrm{cm}^{-3} \cdot \left(\frac{T}{300\mathrm{K}}\right)^{3.2} \end{aligned} \qquad (19)$$

$$\alpha_{n,p} = 0.72 \cdot \left(\frac{T}{300\mathrm{K}}\right)^{0.065} \qquad (20)$$

The fits (18)-(20) are from [19]. Similar data have been provided in [3] and [11].

In view of partial ionization one should consider neutral impurity scattering. However, in view of the uncertainty of the quantitative values for ionized impurity scattering it seems not to be worthwhile to introduce another scattering mechanism with additional fitting parameters.

Particular emphasis has to be put on surface scattering which is modeled with an expression suggested by Seavey [42]

$$\mu_{n,p}^{LIS} = \frac{\mu_{n,p}^{ref} + (\mu_{n,p}^{LI} - \mu_{n,p}^{ref}) \cdot (1 - F(y))}{1 + F(y) \cdot \left(\frac{S_{n,p}}{S_{n,p}^{ref}}\right)^{\gamma_{n,p}}} \qquad (21)$$

with

$$\begin{aligned} \mu_n^{ref} &= 638\,\frac{\mathrm{cm}^2}{\mathrm{Vs}} \cdot \left(\frac{T}{300\mathrm{K}}\right)^{-1.19} \\ \mu_p^{ref} &= 160\,\frac{\mathrm{cm}^2}{\mathrm{Vs}} \cdot \left(\frac{T}{300\mathrm{K}}\right)^{-1.09} \end{aligned}$$

$$F(y) = \frac{2 \cdot \exp\left(-\left(\frac{y}{y^{ref}}\right)^2\right)}{1 + \exp\left(-2 \cdot \left(\frac{y}{y^{ref}}\right)^2\right)}$$

$$S_n = \max\left(0, \frac{\partial\psi}{\partial y}\right), \qquad S_p = \max\left(0, -\frac{\partial\psi}{\partial y}\right) .$$

S_n^{ref} is assumed to be $7 \cdot 10^5\,\frac{\mathrm{V}}{\mathrm{cm}}$, S_p^{ref} is $2.7 \cdot 10^5\,\frac{\mathrm{V}}{\mathrm{cm}}$, γ_n is 1.69, γ_p is 1.0, and y^{ref} is 10 nm. The formulae for surface scattering are definitely not the ultimate expressions. They just fit quite reasonably experimental observations.

Velocity saturation can be modeled with formulae (22). The expression for the electron mobility comes directly from the derivation of the enhanced drift–diffusion model [17]. For the hole mobility the same functional form has been assumed and has been fitted to experimental data.

$$\begin{aligned} \mu_n^{LISF} &= \frac{2\mu_n^{LIS}}{1 + \sqrt{1 + \left(\frac{2 \cdot \mu_n^{LIS} \cdot F_n}{v_n^{sat}}\right)^2}} \\ \mu_p^{LISF} &= \frac{\mu_p^{LIS}}{1 + \frac{\mu_p^{LIS} \cdot F_p}{v_p^{sat}}} \end{aligned} \qquad (22)$$

F_n and F_p are the effective driving forces proposed firstly in [17]

$$\begin{aligned} F_n &= \left|\mathrm{grad}\,\psi - \tfrac{1}{n} \cdot \mathrm{grad}(n \cdot U_{T_n})\right| \\ F_p &= \left|\mathrm{grad}\,\psi + \tfrac{1}{p} \cdot \mathrm{grad}(p \cdot U_{T_p})\right| . \end{aligned} \qquad (23)$$

The used saturation velocities are given by

$$\begin{aligned} v_n^{sat} &= 1.45 \cdot 10^7\,\frac{\mathrm{cm}}{\mathrm{s}} \cdot \sqrt{\tanh\left(\frac{155\mathrm{K}}{T}\right)} \\ v_p^{sat} &= 9.05 \cdot 10^6\,\frac{\mathrm{cm}}{\mathrm{s}} \cdot \sqrt{\tanh\left(\frac{312\mathrm{K}}{T}\right)} . \end{aligned} \qquad (24)$$

The functional form of these fits is after [1], and the experimental data matched are [1], [6], and [5]. An eventual dependence on the crystallographic orientation which one would deduce from [2], [26] is presently not taken into account.

3.2. Modeling Carrier Temperatures

To describe carrier heating properly one has to account for local carrier temperatures $T_{n,p}$ in the current relations. This can be achieved by either solving the hydrodynamic equations [39], or by using a model obtained by series expansions of the solution to the energy conservation equations, e.g. by using the enhanced drift–diffusion model which yields for the carrier temperatures

$$T_{n,p} = T_0 + \frac{2}{3} \cdot \frac{q}{k_B} \cdot \tau_{n,p}^{\epsilon} \cdot (v_{n,p}^{sat})^2 \cdot \left(\frac{1}{\mu_{n,p}^{LISF}} - \frac{1}{\mu_{n,p}^{LIS}}\right) . \qquad (25)$$

The energy relaxation times $\tau^{\epsilon}_{n,p}$ are in the order of 0.5 picoseconds. They should be modeled as functions of the local doping concentration as motivated by the following reasoning: The product of carrier mobility times electronic voltage ($k_B/q \cdot T_{n,p}$) which symbolizes a diffusion coefficient must be a decreasing function with increasing carrier voltage [4]. Its maximum is attained at thermal equilibrium. Therefore, the relation

$$\mu^{LISF}_{n,p} \cdot \frac{k_B \cdot T_{n,p}}{q} \leq \mu^{LIS}_{n,p} \cdot U_{T_0} \qquad (26)$$

must hold. Substituting (25) into (26) and rearranging terms one obtains for the energy relaxation times

$$\tau^{\epsilon}_{n,p} \leq \frac{3}{2} \cdot U_{T_0} \cdot \frac{\mu^{LIS}_{n,p}}{\left(v^{sat}_{n,p}\right)^2} \cdot \qquad (27)$$

In MINIMOS the energy relaxation times are modeled on this basis with a fudge factor γ in the range $[0, 1]$ and a default value of 0.8

$$\tau^{\epsilon}_{n,p} = \gamma \cdot \frac{3}{2} \cdot U_{T_0} \cdot \frac{\mu^{LIS}_{n,p}}{\left(v^{sat}_{n,p}\right)^2} \cdot \qquad (28)$$

For vanishing doping one obtains the maximum energy relaxation times which are at room temperature $\tau^{\epsilon}_{n} = 4.44 \cdot 10^{-13}\,\mathrm{s}$, $\tau^{\epsilon}_{p} = 2.24 \cdot 10^{-13}\,\mathrm{s}$.

4. SIMULATION RESULTS

The coupling of Monte Carlo method and enhanced drift–diffusion model briefly described in section 2.2 has been implemented in MINIMOS in order to justify the efficiency and accuracy of that compound model with respect to ultra small MOS transistors [27]. An n–channel MOSFET with $L_{\mathrm{gate}} = 0.25\,\mu\mathrm{m}$, $t_{\mathrm{ox}} = 5\,\mathrm{nm}$ was simulated at room temperature using the combined technique.

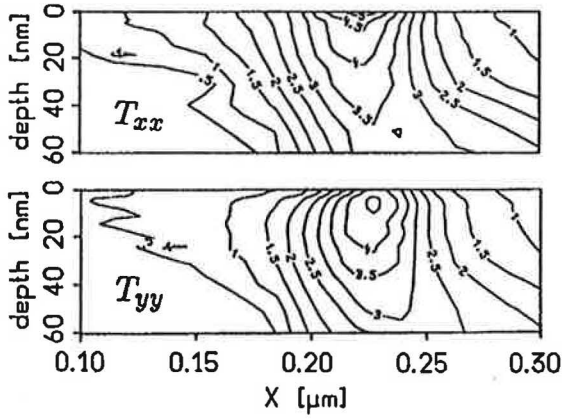

Figure 4: Lateral and transversal temperatures in a quarter micron MOSFET (units [1000 K]).

The device has a metallurgical channel length of $L_{\mathrm{eff}} = 0.15\,\mu\mathrm{m}$ and exhibits a threshold voltage $U_t = 0.23\,\mathrm{V}$. For practical simulation of a MOSFET, electrons are injected in source, where they fully thermalize before entering the channel [40]. In the region of interest, usually near the drain, a sufficient large number of particles is supplied by a particle split algorithm, thus reducing the statistical uncertainty of the results. The bias conditions for the following results are $U_{\mathrm{GS}} = U_{\mathrm{DS}} = 2.5\,\mathrm{V}$ and $U_{\mathrm{BS}} = 0\,\mathrm{V}$.

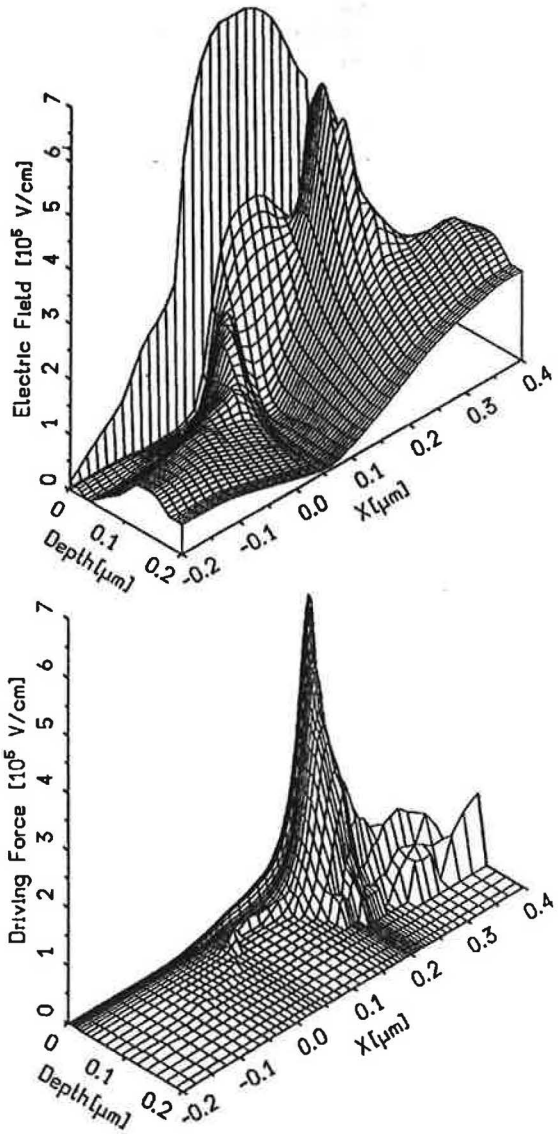

Figure 5: Electric field (upper drawing) and driving force (lower drawing) calculated by Monte Carlo in the same device.

The two–dimensional distribution of the main diagonal temperatures in the area near the drain are depicted in Fig. 4. The lateral temperature T_{xx} has a maximum value at the surface, while the maximum of T_{yy} is shifted away from the surface. Degradation due to hot electron injection into the oxide can be more accurately modeled by using the spatial distribution of T_{yy} than by using the scalar temperature obtained from average energy. In the performed simulations

the off–diagonal temperatures never exceeded 15% of the main–diagonal elements.

Comparing the upper and the lower part of Fig. 5 we see that the large normal field within the inversion layer does not appear in the driving force. This is obvious since the normal field is compensated by diffusion. The electric field in the source junction is compensated by diffusion as well, since in this area the driving force calculated by Monte Carlo vanishes. The field peak near the drain edge however appears almost unchanged in the driving force, thus accelerating and heating up the electron gas in this area.

Velocity of electrons in the channel is plotted in Fig. 6. The effective channel extends from 0.05 μm to 0.2 μm, the positions of the junctions of source and drain subdiffusion, respectively. In the first half of this range the surface velocity (curve A) is lower than the velocities within the inversion layer since the electrons are pressed towards the surface. Near drain the pressing force has opposite direction and the electron velocity is maximum at the surface. The field peak near drain induces a velocity overshoot of 90% related to the bulk saturation velocity. A comparison of the two parts of

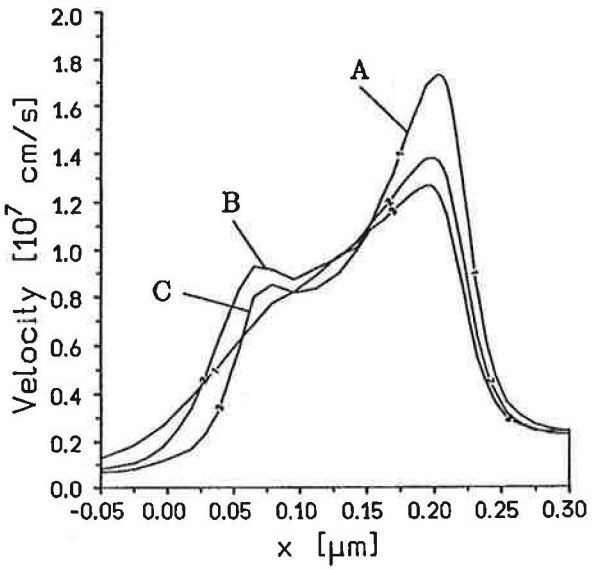

Figure 6: Electron average velocity along the channel. Curve A: at the Si–SiO_2 interface. Curves B and C: 5 nm and 10 nm away from interface.

Fig. 5 has shown that in the overshoot region diffusion is not important. Therefore, velocity overshoot is treated in this model more like a drift phenomenon. It is reproduced by the drift–diffusion current relation (11) by incorporating the nonlocal mobility which will also be increased compared to a local mobility, which cannot produce velocities larger than the bulk saturation velocity.

ACKNOWLEDGEMENTS

Our work is supported by the research laboratories of: AUSTRIAN INDUSTRIES – AMS Int. at Unterpremstätten, Austria; DIGITAL EQUIPMENT Corp. at Hudson, USA; SIEMENS Corp. at Munich, FRG; and SONY Corp. at Atsugi, Japan.

REFERENCES

[1] M. Ali-Omar and L. Reggiani. Drift and Diffusion of Charge Carriers in Silicon and Their Empirical Relation to the Electric Field. *Solid-State Electron. 30*, 7 (1987), 693–697.

[2] M. Aoki, K. Yano, T. Masuhara, S. Ikeda, and S. Meguro. Optimum Crystallographic Orientation of Submicrometer CMOS Devices Operated at Low Temperatures. *IEEE Trans.Electron Devices ED-34*, 1 (1987), 52–57.

[3] N. Arora, J. Hauser, and D. Roulston. Electron and Hole Mobilities in Silicon as a Function of Concentration and Temperature. *IEEE Trans.Electron Devices ED-29* (1982), 292–295.

[4] G. Baccarani and M. Wordeman. An Investigation of Steady-State Velocity Overshoot in Silicon. *Solid-State Electron. 28*, 4 (1985), 407–416.

[5] C. Canali, G. Majni, R. Minder, and G. Ottaviani. Electron and Hole Drift Velocity Measurements in Silicon and Their Empirical Relation to Electric Field and Temperature. *IEEE Trans.Electron Devices ED-22* (1975), 1045–1047.

[6] C. Canali and G. Ottaviani. Saturation Values of the Electron Drift Velocity in Silicon between 300K and 4.2K. *Physics Lett. 32A*, 3 (1970), 147–148.

[7] D. Caughey and R. Thomas. Carrier Mobilities in Silicon Empirically Related to Doping and Field. *Proc.IEEE 52* (1967), 2192–2193.

[8] P. Ciampolini, A. Pierantoni, M. Melanotte, C. Cecchetti, C. Lombardi, and G. Baccarani. Realistic Device Simulation in Three Dimensions. In *Proc.Int.Electron Devices Meeting* (1989), pp. 131–134.

[9] E. Conwell. *High Field Transport in Semiconductors.* Academic Press, 1967.

[10] H. Daembkes, H.-J. Herzog, H. Jorke, H. Kibbel, and E. Kaspar. The n-Channel SiGe/Si Modulation-Doped Field-Effect Transistor. *IEEE Trans.Electron Devices 33*, 5 (May 1986), 633–638.

[11] J. Dorkel and P. Leturcq. Carrier Mobilities in Silicon Semi-Empirically Related to Temperature, Doping and Injection Level. *Solid-State Electron. 24* (1981), 821–825.

[12] I. Gamba and M. Squeff. Simulation of the Transient Behavior of a One-Dimensional Semiconductor Device II. *SIAM J.Numer.Anal. 26*, 3 (1989), 539–552.

[13] H. Gummel. A Self-Consistent Iterative Scheme for One-Dimensional Steady State Transistor Calculations. *IEEE Trans.Electron Devices ED-11* (1964), 455–465.

[14] J. Han, D. Ferry, and P. Newman. Ultra-submicrometer-gate AlGaAs/GaAs HEMT's. *IEEE Electron Device Lett. 11*, 5 (1990), 209–211.

[15] W. Hänsch and H. Jacobs. Enhanced Transconductance in Deep Submicrometer MOSFET. *IEEE Electron Device Lett. EDL-10*, 7 (1989), 285–287.

[16] W. Hänsch and M. Miura-Mattausch. The Hot-Electron Problem in Small Semiconductor Devices. *J. Appl. Phys. 60* (1986), 650.

[17] W. HÄNSCH AND S. SELBERHERR. MINIMOS 3: A MOSFET Simulator that Includes Energy Balance. *IEEE Trans.Electron Devices ED-34*, 5 (May 1987), 1074–1078.

[18] W. HÄNSCH AND W. WEBER. The Effect of Transients on Hot Carriers. *IEEE Electron Device Lett. EDL-10*, 6 (1989), 252–254.

[19] A. HENNING, N. CHAN, J. WATT, AND J. PLUMMER. Substrate Current at Cryogenic Temperatures: Measurements and a Two-Dimensional Model for CMOS Technology. *IEEE Trans.Electron Devices ED-34*, 1 (1987), 64–74.

[20] P. HEREMANS, G. VANDENBOSCH, R. BELLENS, G. GROESENEKEN, AND H. MAES. Temperature Dependence of the Channel Hot-Carrier Degradation of n-Channel MOSFET's. *IEEE Trans.Electron Devices ED-37*, 4 (1990), 980–993.

[21] K. HOFMANN. Charge control in SiGe Quantum-Well MOSFETs and MODFETs. *Mat.Res.Soc.Symp.Proc 220* (1991), 457–463.

[22] C. JACOBONI. Monte Carlo Techniques. In *European School on Device Modeling* (University of Bologna, Italy, March 1991), pp. 101–124.

[23] C. JACOBONI AND L. REGGIANI. The Monte Carlo Method for the Solution of Charge Transport in Semiconductors with Applications to Covalent Materials. *Review of Modern Physics 55*, 3 (1983), 645–705.

[24] D. KAHNG AND M. ATALLA. Silicon-Silicondioxide Field Induced Surface Devices. In *IRE-AIEE Solid-State Device Res.Conf.* (1960).

[25] W. KAUSEL, H. PÖTZL, G. NANZ, AND S. SELBERHERR. Two-Dimensional Transient Simulation of the Turn-Off Behavior of a Planar MOS-Transistor. *Solid-State Electron. 32*, 9 (1989), 685–709.

[26] M. KINUGAWA, M. KAKUMU, T. USAMI, AND J. MATSUNAGA. Effects of Silicon Surface Orientation on Submicron CMOS Devices. In *Proc.Int.Electron Devices Meeting* (1985), pp. 581–584.

[27] H. KOSINA AND S. SELBERHERR. Coupling of Monte Carlo and Drift Diffusion Method with Applications to Metal Oxide Semiconductor Field Effect Transistors. *Jap. J. Appl. Phys. 29*, 12 (December 1990), 2282–2285.

[28] E. LANGER. Numerical Simulation of MOS Transistors. In *IMA Workshop on Semiconductors* (University of Minneapolis, Minnesota, USA, August 1991), pp. 1–29.

[29] S. LAUX AND M. FISCHETTI. Monte-Carlo Simulation of Submicrometer *Si* n-MOSFET's at 77 and 300K. *IEEE Electron Device Lett. EDL-9* (1988), 467–469.

[30] S. LI AND W. THURBER. The Dopant Density and Temperature Dependence of Electron Mobility and Resistivity in n-Type Silicon. *Solid-State Electron. 20* (1977), 609–616.

[31] T. LINTON AND P. BLAKEY. A Fast, General Three-Dimensional Device Simulator and Its Application in a Submicron EPROM Design Study. *IEEE Trans.Computer-Aided Design CAD-8*, 5 (1989), 508–515.

[32] H. LOEB, R. ANDREW, AND W. LOVE. Application of 2-Dimensional Solutions of the Shockley-Poisson Equation to Inversion-Layer M.O.S.T. Devices. *Electron.Lett. 4* (1968), 352–354.

[33] T. MANKU AND A. NATHAN. Physical Modelling of Transport Parameters for Strained Layer p-$Si_{1-x}Ge_x$Devices. In *Proc. SISDEP* (1991), vol. 4, pp. 293–302.

[34] C. MOGLESTUE. A Monte-Carlo Particle Model Study of the Influence of the Doping Profiles on the Characteristics of Field-Effect Transistors. In *NASECODE II Conf.* (1981), pp. 244–249.

[35] D. NAYAK, J. WOO, J. PARK, K.-L. WANG, AND K. MACWILLIAMS. Enhancement Mode Quantum-Well Ge_xSi_{1-x} PMOS. *IEEE Electron Device Lett. 12*, 4 (1991), 154–156.

[36] M. ORLOWSKI AND C. WERNER. Model for the Electric Fields in LDD MOSFET's – Part II: Field Distribution on the Drain Side. *IEEE Trans.Electron Devices ED-36*, 2 (1989), 382–391.

[37] M. ORLOWSKI, C. WERNER, AND J. KLINK. Model for the Electric Fields in LDD MOSFET's – Part I: Field Peaks on the Source Side. *IEEE Trans.Electron Devices ED-36*, 2 (1989), 375–381.

[38] Y. PARK, D. NAVON, AND T. TANG. Monte Carlo Simulation of Bipolar Transistors. *IEEE Trans.Electron Devices ED-31*, 12 (1984), 1724–1730.

[39] M. RUDAN AND A. GNUDI. The Hydrodynamic Model of Current Transport in Semiconductors. In *European School on Device Modeling* (University of Bologna, Italy, March 1991), pp. 125–160.

[40] E. SANGIORGI, B. RICCO, AND F. VENTURI. MOS2: An Efficient MOnte Carlo Simulator for MOS Devices. *IEEE Trans.Computer-Aided Design CAD-7*, 2 (1988), 259–271.

[41] J. SCHROEDER AND R. MULLER. IGFET Analysis Through Numerical Solution of Poisson's Equation. *IEEE Trans.Electron Devices ED-15*, 12 (1968), 954–961.

[42] S. SELBERHERR, W. HÄNSCH, M. SEAVEY, AND J. SLOTBOOM. The Evolution of the MINIMOS Mobility Model. *Solid-State Electron. 33*, 11 (1990), 1425–1436.

[43] S. SELBERHERR AND E. LANGER. Low temperature MOS device modeling. In *Workshop On Low Temperature Semiconductor Electronics* (Burlington, Vermont, 1989), pp. 68–72.

[44] S. SELBERHERR AND E. LANGER. Three dimensional process and device modeling. *Microelectronics Journal 20*, 1-2 (1989), 113–127.

[45] G. SHAHIDI, D. ANTONIADIS, AND H. SMITH. Electron Velocity Overshoot at Room and Liquid Nitrogen Temperatures in Silicon Inversion Layers. *IEEE Electron Device Lett. EDL-9*, 2 (1988), 94–96.

[46] J. SLOTBOOM AND G. STREUTKER. The Mobility Model in MINIMOS. In *ESSDERC* (1989), pp. 87–91.

[47] S. SVENSSON. Theoretical Analysis of the Layer Design of Inverted Single-Channel Heterostructure Transistors. *IEEE Trans.Electron Devices ED-34*, 5 (1987), 992–1000.

[48] C. VAN DE WALLE AND R. MARTIN. Theoretical calculations of heterojunction discontinuities in the Si/Ge system. *Physical Review B 34*, 8 (1986), 271–274.

[49] A. WALKER AND P. WOERLEE. A Mobility Model for MOSFET Device Simulation. In *ESSDERC* (1988), pp. 265–269.

[50] T. WANG AND C.-H. HSIEH. Numerical Analysis of Nonequilibrium Electron Transport in AlGaAs/InGaAs/GaAs Pseudomorhic MODFET's. *IEEE Trans.Electron Devices 37*, 9 (Sept. 1990), 1930–1938.